Simultaneous Raman and Laser Velocimeter Measurements

M. E. HILLARD JR.,* W. W. HUNTER JR.,†
J. F. MEYERS,* AND W. V. FELLER‡
NASA Langley Research Center, Hampton, Va.

Introduction

NONINTRUSIVE flow measurements techniques have received significant attention by those interested in defining flowfield properties. Nondisturbing techniques have been long sought to avoid the uncertainties introduced by the presence of physical probes. In recent years the interest in hypersonic flows prompted development of new techniques such as the electron beam and re-examination and refinement of old techniques such as light absorption techniques. More recently the need for nonintrusive techniques has been further stimulated by increased research of three-dimensional flowfields for the supersonic and transonic flow regimes.

Development of the laser velocimeter[1,2] and Raman[3,4] scattering techniques has provided unique methods for defining the fluid mechanic structure of three-dimensional flowfields. The laser velocimeter inherently provides velocity vector information. The Raman technique provides measurements of local static density and temperature and is not flow direction sensitive. Both techniques provide local "point" measurements. Combined, these techniques offer the potential of local nondisturbing simultaneous measurements of the three basic gas parameters, i.e., velocity, density, and temperature, necessary to define the thermodynamic state of the fluid.

The purpose of the work reported here was to demonstrate the feasibility of combined measurements with LV and Raman scattering. Because of the vast differences in the cross sections associated with Mie ($\simeq 10^{-10}$ cm^2/sterad) and Raman ($\simeq 10^{-30}$ cm^2/sterad) scattering, which are fundamental to the laser velocimeter and Raman techniques, respectively, several considerations were evaluated experimentally. First, would the background radiation associated with the Mie scattering swamp out the Raman signals? Second, would the Raman spectra of the particulate material significantly contaminate the Raman air spectra? With these goals in mind a series of experiments was conducted in a Mach 5 facility operated at a nominal stagnation pressure and temperature of 3.45×10^4 N/m^2 (50 psia) and 375 K (675°R). Measurements were made in the inviscid flowfield before and about a sharp leading-edge flat-plate model. The measured mean values of static temperature, static density, and $\bar{u}$ velocity vector ranged from 70.0 to 75.9K, 4.31×10^{-2} to 6.29×10^{-2} kg/m^2, and 755 to 777 m/sec, respectively. These values were compared with calculated values based on pitot pressure, static pressure along the flat-plate model, and stagnation chamber measurements.

Experimental Apparatus

A schematic diagram of the combined laser velocimeter (LV) and Raman apparatus is shown in Fig. 1. Two lasers, operated at different wavelengths, were used in these tests. It is expected that a single laser with optimum optics would provide sufficient incident radiation power. Both lasers were argon-ion cw devices with the LV channel operated at 514.5 nm and the Raman channel operated at 488.0 nm with an approximate output power of 1.4 w for each.

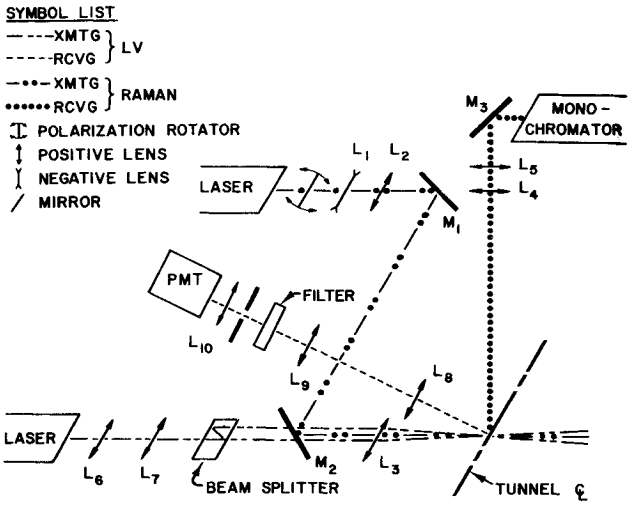

Fig. 1 Schematic diagram of the LV/Raman optical apparatus.

The Raman channel radiation was directed to the desired measurement position in the test section by a beam expander (lenses L_1 and L_2) and a focusing lens (L_3). Both the Raman and LV channels passed through the standard tunnel schlieren window and were collected in a light trap. The Raman measurement volume was 6 mm in length and 0.1 mm in diameter and was centered on the model centerline. The light scattered in the Raman measurement volume was collected perpendicular to the laser beam by lens L_4 (f/5), directed into a double monochromator by lens L_5, and detected by a photon-counting system.

The LV channel radiation was directed to the measurement position in the test section through lenses L_6 and L_7, optical beam splitter, and the common focusing lens L_3. Mirror M_3 contained clearance holes for passage of the parallel LV beams to lens L_3. The LV sample volume scattered light which was collected and directed by lenses L_8 and L_9 to a spatial filter with a 1.5-mm-diam aperture. Lens L_{10} collected and directed light from the aperture to the photomultiplier detector. The interference filter function was to reject 488.0 nm light thereby reducing LV system background noise. The LV receiving optics were set at a 15° angle in the same plane as the transmitting LV optics. The LV measurement volume was 20 mm long and 1.2 mm in diameter and was centered with the Raman measurement volume. The LV signal was processed through a digital frequency counter system with 25 MHz reference clock.

The flat-plate model was 66 mm long and 25 mm wide and was instrumented with five static pressure orifices placed approximately 13 mm apart along the centerline. A pitot tube was located approximately 3 mm above and 45 mm behind the leading edge on the plate centerline. Additional measurements of the test chamber static pressure, the nozzle-exit static pressure, and the nozzle stagnation pressure and temperature were recorded.

The test facility is a 10.7-cm-diam, Mach 5, freejet contained in a chamber. The nozzle is supplied from a high pressure air tank and exhausts downstream through a diffuser to a vacuum sphere. The seeding particles, required by the LV, were generated by a vaporization-recondensing smoke generator that fed into the supply pipe upstream of the stagnation chamber. The seeding material, Dow Corning 704 diffusion pump oil, was mixed with air and vaporized in a small bore tube surrounding a cal rod heater. The expansion of the vapor at the tube exit caused rapid cooling, condensing the oil into small particles.

Measurement Technique

The Raman effect is an inelastic light-scattering process where the frequency of the scattered light is shifted from that of the

Received April 5, 1974.
Index categories: Supersonic and Hypersonic Flow; Lasers; Research Facilities and Instrumentation.

* Aero-Space Technologist, Gas Parameters Measurements Section, Instrument Research Division.
† Aero-Space Technologist, Head, Gas Parameters Measurements Section, Instrument Research Division. Member AIAA.
‡ Aero-Space Technologist, Gas Dynamics Section, Hypersonic Vehicles Division.

incident light by an amount which depends on the structure of the scattering gas molecules. The intensity and intensity variations in the scattered-light spectrum can be directly related to the gas molecular density and temperature.

The static temperature was determined herein by ratioing the intensities of two pure rotational Raman lines of nitrogen. The relationship for the temperature T is given by

$$T = \frac{H}{\ln(R/G)}$$

H and G are constants which are determined by the specified transitions used and R is the intensity ratio. The transitions used were the $J = 6$ to $J = 4$ anti-Stokes transition (6, 4) and the $J = 1$ to $J = 3$ Stokes transition (1, 3) of nitrogen where J is the rotational quantum number. These transitions were chosen because they could be easily separated from the remaining Raman spectrum of air and because they provided good temperature sensitivity in the range of interest, 60–100K.

To obtain the temperature measurement, a 1 cm^{-1} spectral bandpass was used and the monochromator was positioned on the (6, 4) transition (which is shifted 44 cm^{-1} above the laser line). The intensity of this transition was monitored and the procedure was repeated on the (1, 3) transition (which is shifted 20 cm^{-1} below the laser line). An integration time of 1 sec was used for both the temperature and density measurements.

The density measurements were obtained by monitoring the intensity of the (6, 4) transition. The temperature effect on the (6, 4) transition was eliminated by using the Raman measured static temperature to correct the measured intensity of the (6, 4) transition for static temperature variations. This eliminated the temperature dependence and the resulting intensity of the (6, 4) transition was directly proportional to gas density. By utilizing this approach for the static density measurements, only two measurements were necessary to obtain static temperature and density: the intensities of the (6, 4) and (1, 3) transitions.

The laser velocimeter is functionally dependent on elastic scattering of light, i.e., Mie scattering. The particular form of the LV system used in this work split the 514.5 nm beam into two approximately equal intensity parallel beams. These beams are focused and crossed at the location of interest in the flowfield. Wavefronts of each beam are coherent with respect to each other and form a series of interference fringes in the test volume. Small particles, or seeds, embedded in the flow scatter light upon passage through the fringe field. The intensity of the scattered light varies as a function of the particle position in the test volume. Frequency f of the intensity variation is a function of the fringe spacing and particle velocity, u. The relation is given by

$$f = (2u/\lambda)\sin(\theta/2)$$

where λ is the incident radiation wavelength and θ is the cross beam angle. Measured frequencies obtained from the frequency counter were collected and stored in a pulse height analyzer. A sufficient number of data points were collected to define a mean Doppler frequency and frequency distribution. Mean velocity values and a standard deviation were calculated from these data.

The calculated temperature (T calc), density (ρ calc), and velocity (u calc) were based on the local Mach number, estimated from the static pressure distribution on the flat-plate and pitot pressure measurements, and the stagnation chamber pressure and temperatures. Mach number error is estimated to be less than 1%.

Results and Discussion

Results of simultaneous Raman and LV measurements are given in Table 1 and calculated values are also indicated for comparison. One standard deviation, $\Delta\rho$, ΔT, and Δu associated with the measured values are also shown. In general the agreement between the measured and calculated values is good.

Raman mean temperature values are based on the average of six 10-sec measurements of each rotational transition (6, 4 and 1, 3) and the mean density is based on the measured average value of the 6, 4 rotational transition. Of course all Raman density measurements were normalized to the input laser power and a system calibration was performed before each tunnel run. An increase in the background level for the Raman measurements due to the seeding particulates was detected; however the increase was not prohibitive. Measurements of background radiation were made and measured intensity corrected.

Table 1 Comparison of results of LV/Raman measurements with calculated values

ρ_{Raman}	$\Delta\rho$	ρ_{calc}	T_{Raman}	ΔT	T_{calc}	u_{LV}	Δu	u_{calc}
$(kg/m^3) \times 10^2$			(K)			(m/sec)		
4.31	0.55	4.37	70.0	3.8	68.3	620	147	792
6.29	0.60	6.32	75.9	4.2	74.7	755	125	755
4.20	0.59	4.32	59.9	4.3	62.7	755	118	769
6.21	0.59	6.50	73.2	3.5	72.4	777	136	743

Laser velocimeter measurements were based on approximately a million measured events which occurred at a rate of about 2×10^4 per sec. Measurement results agree well with the calculated values except in one instance. This one significant deviation is attributed to the seeding generator yielding a particle size distribution with a large mean value. These large particles lag the flow to an extent that they still have not obtained the flow velocity when they reach the LV sample volume, approximately 55 cm downstream of the nozzle throat. The seeding generator was adjusted for the subsequent tests to yield a small particle size, thus resulting in measurements with better agreement with the calculated velocity values. The large standard deviation Δu is due to two factors. The first is that the particle size distribution was quite broad, yielding a significant number of large particles which lagged the flow, even though the mean particle size was small. This had the effect of broadening the velocity distribution toward the lower velocities. Second, the frequency counter determines the number of whole clock pulses that occur and during round off yields a lower time value than the actual time for eight cycles, which gives a bias toward higher signal frequencies and thus higher velocities. The amount of bias is inversely proportional to the clock frequency. Since the clock frequency was only approximately 2.25 times the signal frequency, this bias was quite large. This had the effect of broadening the velocity distribution toward the higher velocities.

Conclusions

The present investigation has demonstrated that Raman and laser velocimeter measurements can be made simultaneously and that the background due to a large particulate concentration did not saturate or distort the relatively weak rotational Raman signals.

Under stringent conditions of low static gas densities and large particulate concentrations Raman density and temperature measurements agree to within $\pm 5\%$ of the calculated values. The large standard deviation of the laser velocimeter measurements of these tests is not typical, but was due to adapting a low pressure smoke generator to a high pressure situation which compromised its capabilities for yielding a narrow size distribution and not using a higher frequency clock in the LV frequency counter. The correction of both situations will yield velocity measurements with a much lower uncertainty.

References

[1] Foreman, J. W., Jr., George, E. W., and Lewis, R. D., "Measurement of Localized Flow Velocities in Gases with a Laser Doppler Flowmeter," *Applied Physics Letters*, Vol. 7, No. 4, Aug. 15, 1965, pp. 77–78.

[2] Brayton, D. B., "A Laser Doppler-Shift, Velocity Meter with Self-Aligning Optics," *Proceedings of the Electro-Optical Systems Design Conference*, Industrial and Scientific Conference Management Inc.,New York, Sept. 16–18, 1969, pp. 168–177.

[3] Widhopf, G. F. and Lederman, S., "Specie Concentration Measurements Utilizing Raman Scattering of a Laser Beam," *AIAA Journal*, Vol. 9, No. 2, Feb. 1971, pp. 309–316.

[4] Bandy, A. R., Hillard, M. E., and Emory, L. E., "Evaluation of Raman Scattering as a Sensor of Temperature and Molecular Density," *Applied Spectroscopy*, Vol. 27, No. 6, Nov./Dec. 1973, pp. 421–424.

Numerical Solution of Transonic Flows about Quasi-Cylindrical Configurations

ANTONIO FERRI,* SHELDON ELZWEIG,†
AND
PAOLO BARONTI‡
Advanced Technology Laboratories, Inc., Westbury, N.Y.

Introduction

NUMERICAL solutions of three-dimensional flows are lengthy and costly. A numerical algorithm is presented which allows for a fast solution of the transonic flow about quasi-cylindrical configurations of arbitrary shape. The method is conceptually similar to that developed by A. Ferri,[1] for conical flowfields without axial symmetry at supersonic speed.

Analysis

In order to describe the method, we consider the transonic small disturbance equation in terms of the perturbation potential and assume a configuration with one plane of symmetry. In a polar coordinate system, where the angle θ is zero in the vertical direction, the problem is described by the equation

$$[1-M_\infty{}^2-M_\infty{}^2(\gamma+1)\Phi_x]\Phi_{xx}+\Phi_{rr}+(1/r)\Phi_r=-(1/r^2)\Phi_{\theta\theta} \quad (1)$$

with the boundary condition, along a cylindrical surface $r=R$, $\phi_r(x,R,\theta)=(d/dx)r(x,\theta)$, where $r(x,\theta)$ has the general form

$$r(x,\theta)=\sum_0^n a_n(x)\cos n\theta \quad (2)$$

At infinity, the boundary condition is prescribed by either specifying the potential Φ or the proper normal Φ derivatives.

Express now the potential Φ as

$$\Phi(x,r,\theta)=\Phi_0(x,r)+\Phi_1(x,r)\cos\theta+\Phi_2(x,r)\cos 2\theta+\Phi_3(x,r)\cos 3\theta+\cdots \quad (3)$$

and rewrite Eq. (1) in the form

$$[1-M_\infty{}^2-M_\infty{}^2(\gamma+1)\Phi_x]\Phi_{xx}+\Phi_{rr}+(1/r)\Phi_r=(1/r^2)[\Phi_1\cos\theta+4\Phi_2\cos 2\theta+9\Phi_3\cos 3\theta+\cdots]$$

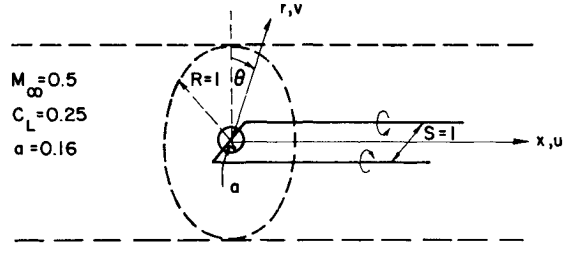

Fig. 1 Coordinates system and schematic configuration.

Received April 15, 1974; revision received June 3, 1974. This work is part of a continuing effort on wall corrections of transonic wind tunnels sponsored jointly by ONR and AFOSR under Contract N00014-72-C-0201. M. Cooper and M. Rogers are monitoring the work.

Index category: Subsonic and Transonic Flow.

* Technical Director; also Astor Professor, New York University. Fellow AIAA.

† Research Scientist.

‡ Senior Research Scientist. Member AIAA.

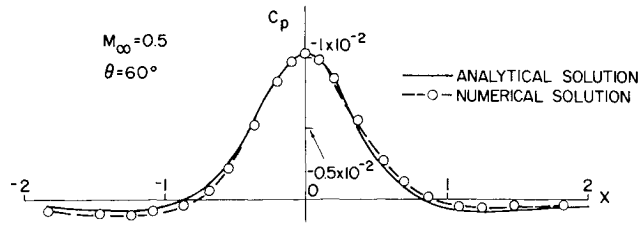

Fig. 2 Analytical and numerical solution of pressure distribution along a typical meridian plane.

This equation is then evaluated at selected θ_i planes so as to obtain the i equations

$$[1-M_\infty{}^2-M_\infty{}^2(\gamma+1)\Phi_x(x,r,\theta_i)]\Phi_{xx}(x,r,\theta_i)+\Phi_{rr}(x,r,\theta_i)+(1/r)\Phi_r(x,r,\theta_i)=(1/r^2)[\Phi_1\cos\theta_i+4\Phi_2\cos 2\theta_i+9\Phi_3\cos 3\theta_i+\cdots] \quad (4)$$

When the quantities $\Phi_1,\Phi_2,\Phi_3,\ldots$ are known, each equation, in each θ_i plane, corresponds to the usual two-dimensional transonic equation with a forcing term on the right-hand side and thus can be solved with any of the numerical schemes already developed for two-dimensional transonic flows. However, the quantities $\Phi_1,\Phi_2,\Phi_3,\ldots$ can be determined within the framework of the numerical relaxation procedures developed for the two-dimensional problem. Let us postulate that $\Phi_1,\Phi_2,\Phi_3,\ldots$ are those calculated at a preceding relaxation step, that is, $\Phi_1{}^{\nu-1},\Phi_2{}^{\nu-1},\Phi_3{}^{\nu-1},\ldots$, where ν indicates the previous iteration. Equation (4) can then be numerically solved in each θ_i plane at the νth iteration. Once this equation has been solved and the $\Phi_i{}^\nu(x,r,\theta_i)$ values determined, the Fourier expansion of Φ, Eq. (3), is written in the form

$$\Phi_i{}^\nu(x,r,\theta_i)=\Phi_0{}^\nu(x,r)+\Phi_1{}^\nu(x,r)\cos\theta_i+\Phi_2{}^\nu(x,r)\cos 2\theta_i+\Phi_3{}^\nu(x,r)\cos 3\theta_i+\cdots$$

and solved at the several θ_i planes to yield a system of i linear algebraic equations in the i unknowns $\Phi_0{}^\nu(x,r),\Phi_1{}^\nu(x,r),\Phi_2{}^\nu(x,r),\Phi_3{}^\nu(x,r),\ldots$. These values are used for the solution of Eq. (4) in the subsequent iteration and the process continued until convergence. In conclusion, the solution of the transonic three-dimensional problem is reduced to the solution of i uncoupled two-dimensional transonic equations with a large reduction of computational time. The number i of two-dimensional equations to be solved is obviously equal to the number of terms that are retained in the Fourier series expansion of Φ. In turn, this number is dictated by the geometry of the body being considered, Eq. (2).

The solutions of the two-dimensional equations, in the θ_i planes, for both subcritical and supercritical conditions are obtained by a numerical program developed at Advanced

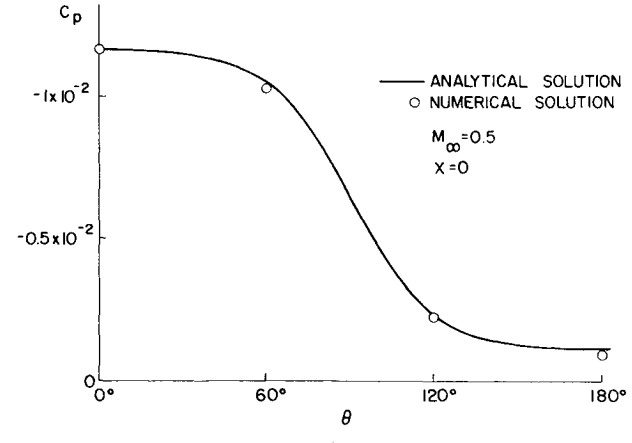

Fig. 3 Analytical and numerical solution of pressure distribution in a circumferential direction.